This figure "fig1.jpg" is available in "jpg" format from:

http://arXiv.org/ps/cond-mat/0111453v1

Possibility between earthquake and explosion seismogram differentiation by discrete stochastic non-Markov processes and local Hurst exponent analysis

Renat Yulmetyev[1] *, Fail Gafarov[1]†, Peter Hänggi[2], Raoul Nigmatullin[3] and Shamil Kayumov[3]
[1]*Department of Theoretical Physics, Kazan State Pedagogical University, Mezhlauk Street, 1 420021 Kazan, Russia*
[2]*Department of Physics, University of Augsburg, Universitätsstrasse 1,D-86135 Augsburg, Germany*
[3]*Department of Physics, Kazan State University, Kremlevskaya Str. 18, 420018, Kazan, Russia*

The basic purpose of the paper is to draw the attention of researchers to new possibilities of differentiation of similar signals having different nature. One of examples of such kind of signals is presented by seismograms containing recordings of earthquakes (EQ's) and technogenic explosions (TE's). EQ's are among the most dramatic phenomena in nature. We propose here a discrete stochastic model for possible solution of a problem of strong EQ's forecasting and differentiation of TE's from the weak EQ's. Theoretical analysis is performed by two independent methods: with the use of statistical theory of discrete non-Markov stochastic processes (Phys. Rev. E **62**,6178 (2000)) and the local Hurst exponent. The following earth states have been considered among them: before (Ib) and during (I) strong EQ, during weak EQ (II) and during TE (III), and in a calm state of Earth core (IV). The estimation of states I, II and III has been made on the particular examples of Turkey (1999) EQ 's, state IV has been taken as an example of underground TE. Time recordings of seismic signals of the first four dynamic orthogonal collective variables, six various plane of phase portrait of four dimensional phase space of orthogonal variables and the local Hurst exponent have been calculated for the dynamic analysis of states of systems I-IV. The analysis of statistical properties of seismic time series I -IV has been realized with the help of a set of discrete time-dependent functions (time correlation function and first three memory functions), their power spectra and first three points in statistical spectrum of non-Markovity. In all systems studied we have found out bizarre combination of the following spectral characteristics: the fractal frequency spectra adjustable by phenomena of usual and restricted self-organized criticality, spectra of a white and color noises and unusual alternation of Markov and non-Markov effects of long range memory, detected earlier (J.Phys.A **27**, 5363(1994)) only for hydrodynamic systems. Our research demonstrates that discrete non-Markov stochastic processes and long- range memory effects play a crucial role in the behavior of seismic systems I -IV. The approaches, permitting to obtain an algorithm of strong EQ's forecasting and to differentiate TE's from weak EQ's, have been developed.

PACS numbers:0.5.65.+b, 02.50.-y, 05.40.-a, 05.65.+b, 45.65.+k

I. INTRODUCTION

The earthquakes are among the most mysterious and dramatic phenomena, occurring in nature. As a result of sets and breakups of terrestrial cortex or higher part of mantle over hundreds of thousands underground pushes and fluctuations of the Earth surface occur annually. They propagate over long distances in the form of elastic seismic waves. Nearly thousands of them are registered by people. Annually nearly hundred earthquakes cause catastrophic consequences: they affect big communities of people and lead to great economical losses.

For the study of basic mechanisms underlying its nature modern numerical and statistical methods are used now in modeling and understanding of the EQ phenomenon. In papers [1], [2] the modified renormalization group theory with complex critical exponents has been studied for implications of EQ's predictions. Long-periodic corrections found fit well the experimental data. Then universal long-periodic corrections based on the modified renormalization group theory have been used successfully [3] for possible predictions of the failure stress phenomenon foregoing an EQ. The failure stress data are in a good reliability with acoustic emission measurements. In paper [4] it has been shown that the log-periodic corrections are of general nature, they are related to the discrete scale invariance and complex fractal dimension. This idea has been checked in [5], [6] for diffusion-limited-aggregate clusters. The paradox of the expected time until the next EQ with an attempt of finding of acceptable distribution is discussed in [7]. New explanation

*e-mail:rmy@dtp.ksu.ras.ru
†e-mail:gfm@dtp.ksu.ras.ru

of Guttenberg-Richter power law related to the roughness of the fractured solid surfaces has been outlined in [8]. Recent achievements and progress in understanding of the complex EQ phenomena from different points of view are discussed in the recent review [9]. New numerical methods like wavelets and multi-scale singular-spectrum analysis in treatment of seismic data are considered in [10].

All these previous methods are developed for understanding the statistical and non- stationary properties of EQ's and TE's. But in this paper we would like to demonstrate some possibilities related initially to differentiation of EQ's from TE's. This problem has not only scientific significance related with recognition of similar signals having physical origin. In recent time it was related also with some political problems associated with testing of nuclear explosions also.

Seismic data are an object of careful analysis and numerous methods of their treatment are used especially for forecasting of EQ's with strong magnitudes. In spite of wide application of approaches based on nonlinear dynamics methods, the Fourier and wavelet transformations etc., we have essential limitations, which narrow down the range of applicability of the results obtained. One of the main difficulty is that the discrete character of the seismic signals registration is not taken into account. Another factor, which should be taken into account is related to the influence of local time effects. Alongside with of the discreteness and the local behavior of the seismic signals considered here exist the third peculiarity, viz., the influence of long-range memory effects.

In this paper, we present one of the possible solutions to forecasting strong EQ's and differentiating TE's from weak EQ's. In this presentation we consider of three important factors for seismic signals registered in the form of seismograms : discreteness, long- range memory and local time behavior. Two new methods are used to analyse these three factors. The first one is based on seismograms considered in the form of a discrete non-Markov statistical process along with analysis of corresponding phase portraits, memory functions and the non-Markovity parameters. The second method is based on the generalized conception of the Hurst exponent. These methods have been used for careful analysis of seismic data and to differentiate EQ's from TE's . The results obtained with the use of these methods are useful in recognition of specific features of EQ's and TE's and can be used for strong EQ's forecasting.

The paper is organized as follows. In Section 2 we describe in brief the stochastic dynamic of time correlation in complex systems containing seismic signals by the discrete non-Markov kinetic equations. The local fractal dimension and the corresponding Hurst exponent are defined in the Section 3. The real data treatment with the use of non-Markov conceptions has been realized in the Section 4. The Section 5 contains some results obtained by the local Hurst exponent method. The basic conclusions are discussed in the final Section 6.

II. THE KINETIC DESCRIPTION OF DISCRETE NON-MARKOV RANDOM PROCESSES

In recent paper [11] the statistical theory of discrete non-Markov random processes has been developed. The basic elements, which are necessary for understanding of other sections, are presented, in brief, here. In accordance with the Refs. [11]- [13] the fluctuations of random variable $\delta x_j = \delta x(T + j\tau), j = 0, 1, \cdots, N-1$ of a complex system can be represented as k-component state vector

$$\mathbf{A}_k^0(0) = (\delta x_0, \delta x_1, \delta x_2, \cdots, \delta x_{k-1}) = (\delta x(T), \delta x(T+\tau), \cdots, \delta x(T+(k-1)\tau). \tag{1}$$

Here τ is a finite discretization time, δx_j and $< x >$ define fluctuations and mean value correspondingly, T is the beginning of the time series. They are defined by conventional relationships

$$\delta x_j = x_j - < x >, \ < x >= \frac{1}{N}\sum_{j=0}^{N-1} x(T + j\tau). \tag{2}$$

The set of state vectors forms a finite-dimensional Euclidean space, where the scalar product of two vectors can be defined as

$$< \mathbf{A} \cdot \mathbf{B} >= \sum_{j=0}^{k-1} A_j B_j. \tag{3}$$

The time dependence of the vector $\mathbf{A}$ can be defined as result of discrete m-step shift

$$\mathbf{A}_{m+k}^m(t) = \{\delta x_m, \delta x_{m+1}, \delta x_{m+2}, \cdots, \delta x_{m+k-1}\}$$
$$= \{\delta x(T + m\tau), \delta x(T + (m+1)\tau), \delta x(T + (m+2)\tau), \cdots, \delta x(T + (m+k-1)\tau\}, \tag{4}$$

where $t = m\tau$ and τ is a finite time step. Statistical parameters (absolute and relative variances) can be expressed by means of the scalar product of two vectors as following

$$\sigma^2 = \frac{1}{N} < \mathbf{A}_N^0 \cdot \mathbf{A}_N^0 >= N^{-1}\{\mathbf{A}_N^0\}^2,$$
$$\delta^2 = \frac{< \mathbf{A}_N^0 \cdot \mathbf{A}_N^0 >}{N < X >^2}.$$

We define the evolution operator for the description of evolution of the variables δx_j as following

$$\delta x_{j+1}(T + (j+1)\tau) = U(T + (j+1)\tau, T + j\tau)\delta x_j(T + j\tau) = U(\tau)\delta x_j. \tag{5}$$

One can write formally the discrete equation of motion by the use of operator $U(\tau)$ in the form

$$\frac{\Delta x(t)}{\Delta t} = \frac{x(t+\tau) - x(t)}{\tau} = \frac{1}{\tau}\{U(t+\tau, t) - 1\}x(t). \tag{6}$$

The normalized time correlation function (TCF) can be represented by Eqns. (1) and (4) (where $t = m\tau$ is current discrete time) as follows

$$a(t) = \frac{< \mathbf{A}_k^0 \cdot \mathbf{A}_{m+k}^m >}{< \mathbf{A}_k^0 \cdot \mathbf{A}_k^0 >} = \frac{< \mathbf{A}_k^0(0) \cdot \mathbf{A}_{m+k}^m(t) >}{< \mathbf{A}_k^0(0)^2 >}. \tag{7}$$

From the last equation (7) one can see that TCF $a(t)$ is obtained by projection of the final state vector $\mathbf{A}_{m+k}^m(t)$ (4) on the initial state vector $\mathbf{A}_k^0(0)$. Because of this property one can write the projection operator in the linear space of state vectors

$$\Pi \mathbf{A}_{m+k}^m(t) = \mathbf{A}_k^0(0)\frac{< \mathbf{A}_k^0(0)\mathbf{A}_{m+k}^m(t) >}{< |\mathbf{A}_k^0(0)|^2 >} = \mathbf{A}_k^0(0)a(t). \tag{8}$$

The projection operator Π has the following properties

$$\Pi = \frac{|\mathbf{A}_k^0(0) >< \mathbf{A}_k^0(0)|}{< |\mathbf{A}_k^0(0)|^2 >}, \quad \Pi^2 = \Pi, \quad P = 1 - \Pi, \quad P^2 = P, \quad \Pi P = 0, P\Pi = 0. \tag{9}$$

The projection operators Π and P are idempotent and mutually complementary. Projector Π projects on the direction of initial state vector $\mathbf{A}_k^0(0)$, while the projector P projects all vectors on the direction which is orthogonal to the previous one. Let us apply the projection technique in the state vectors space for deduction of the discrete finite-difference Liouville's equation

$$\frac{\Delta}{\Delta t}\mathbf{A}_{m+k}^m(t) = i\hat{L}(t,\tau)\mathbf{A}_{m+k}^m(t), \tag{10}$$
$$\hat{L}(t,\tau) = (i\tau)^{-1}\{U(t+\tau, t) - 1\}.$$

The first expression defines the Liouville's quasioperator $\hat{L}$ and the second expression defines the evolution operator $U(t)$. Transferring from vectors $\mathbf{A}_{m+k}^m$ to a scalar value of the TCF $a(t)$ by means of suitable projection procedure one can obtain the closed finite-difference equation for the initial TCF

$$\frac{\Delta a(t)}{\Delta t} = \lambda_1 a(t) - \tau\Lambda_1 \sum_{j=0}^{m-1} M_1(j\tau)a(t - j\tau). \tag{11}$$

Here Λ_1 is the relaxation parameter while the frequency λ_1 defines the eigen spectrum of the Liouville's quasioperator $\hat{L}$ in the following way

$$\lambda_1 = i\frac{< \mathbf{A}_k^0(0)\hat{L}\mathbf{A}_k^0(0) >}{< |\mathbf{A}_k^0(0)|^2 >}, \quad \Lambda_1 = \frac{< \mathbf{A}_k^0\hat{L}_{12}\hat{L}_{21}\mathbf{A}_k^0(0) >}{< |\mathbf{A}_k^0(0)|^2 >}. \tag{12}$$

The standard Liouville's equation is obtained easily from Eqs. (6), (10) by means of the limit $\tau \to 0$. In this case the Liouville's quasioperator $\hat{L}$ is reduced to a classical or quantum Liouvillian and is defined correspondingly by the

classical or quantum Hamiltonian of the system considered. The given approach is true for non-Hamiltonian systems of arbitrary nature when the Hamiltonian cannot be written together with conventional equations of motion. The function $M_1(j\tau)$ in the right hand side of Eqn. (11) is the first order memory function

$$M_1(j\tau) = \frac{< \mathbf{A}_k^0(0)\hat{L}_{12}\{1 + i\tau\hat{L}_{22}\}^j\hat{L}_{21}\mathbf{A}_k^0(0) >}{< \mathbf{A}_k^0(0)\hat{L}_{12}\hat{L}_{21}\mathbf{A}_k^0(0) >}, \quad M_1(0) = 1. \tag{13}$$

Here we use the following notation for the matrix elements of the splittable Liouvillian quasioperator $L_{i,j} = \Pi_i\hat{L}\Pi_j$, $i = 1, 2$, $\Pi_1 = \Pi$, $\Pi_2 = P$, $\hat{L}_{11} = \Pi\hat{L}\Pi$, $\hat{L}_{12} = \Pi\hat{L}P$, $\hat{L}_{21} = P\hat{L}\Pi$, $\hat{L}_{22} = P\hat{L}P$. Equation (11) can be considered as the first equation of the finite-difference kinetic equations chain with memory for the discrete TCF $a(t)$. In paper [11] it has been demonstrated that using Gramm-Schmidt orthogonalization procedure one can define the dynamic orthogonal variables $\mathbf{W}_n(t)$ by means of the following recurrence relationships

$$\mathbf{W}_0 = \mathbf{A}_k^0(0), \quad \mathbf{W}_1 = \{i\hat{L} - \lambda_1\}\mathbf{W}_0, \quad \mathbf{W}_n = \{i\hat{L} - \lambda_{n-1}\}\mathbf{W}_{n-1} + \Lambda_{n-1}\mathbf{W}_{n-2}, \quad n > 1. \tag{14}$$

Here we introduce the fundamental eigen values λ_n and relaxation Λ_n parameters as follows

$$\lambda_n = i\frac{< \mathbf{W}_n\hat{L}\mathbf{W}_n >}{< |\mathbf{W}_n|^2 >}, \quad \Lambda_n = -\frac{\langle \mathbf{W}_{n-1}(i\hat{L} - \lambda_{n+1})\mathbf{W}_n\rangle}{\langle|\mathbf{W}_{n-1}|^2\rangle} \ . \tag{15}$$

Parameters λ_n are very similar to the Lyapunov's exponents. Arbitrary orthogonal variables $\mathbf{W}_n$ can be expressed directly via the initial variable $\mathbf{W}_0 = \mathbf{A}_k^0(0)$ by means of (14) in the generalized form

$$\mathbf{W}_n = \begin{vmatrix} (i\hat{L} - \lambda_1) & \Lambda_1^{1/2} & 0 & \dots & 0 \\ \Lambda_1^{1/2} & (i\hat{L} - \lambda_2) & \Lambda_2^{1/2} & \dots & 0 \\ 0 & \Lambda_2^{1/2} & (i\hat{L} - \lambda_3) & \dots & 0 \\ 0 & 0 & 0 & \dots & (i\hat{L} - \lambda_{n-1}) \end{vmatrix} \mathbf{W}_0. \tag{16}$$

The physical sense of the new variables $\mathbf{W}_n$ can be interpreted as follows. For example, the local density of fluctuations in the physics of continuous media can be identified with the initial variable $\mathbf{W}_0$. In this case the fluctuations of the local current density, local energy density and local energy current density can be associated with the dynamic variables $\mathbf{W}_n$ with numbers $n = 1, 2, 3$, correspondingly.

One can relate to the set of projection operators Π_n to the set of orthogonal variables (14). The last ones project an arbitrary dynamic variable (viz., a state vector) Y on the corresponding initial state vector $\mathbf{W}_n$

$$\Pi_n = \frac{|\mathbf{W}_n >< \mathbf{W}_n^*|}{< |\mathbf{W}_n|^2 >}, \quad \Pi_n^2 = \Pi_n, \quad P_n = 1 - \Pi_n, \quad P_n^2 = P_n, \quad \Pi_n P_n = 0,$$
$$\Pi_n\Pi_m = \delta_{n,m}\Pi_n, \quad P_nP_m = \delta_{n,m}P_n, \quad P_n\Pi_n = 0. \tag{17}$$

Acting successively by projection operators Π_n and P_n on the finite-difference equations (10) for the normalized discrete memory functions

$$M_n(t) = \frac{< \mathbf{W}_n[1 + i\tau\hat{L}_{22}^{(n)}]^m\mathbf{W}_n >}{< |\mathbf{W}_n(0)|^2 >} \tag{18}$$

one can obtain a chain of the coupled non-Markov finite-difference kinetic equations of the following type

$$\frac{\Delta M_n(t)}{\Delta t} = \lambda_{n+1}M_n(t) - \tau\Lambda_{n+1}\sum_{j=0}^{m-1} M_{n+1}(j\tau)M_n(t - j\tau) \ , \tag{19}$$

Here λ_n is the eigen value spectrum of Liouville's operator $i\hat{L}$, while Λ_n is the general relaxation parameters,

$$\lambda_n = i\frac{< \mathbf{W}_n^*L\mathbf{W}_n >}{< |\mathbf{W}_n|^2 >}, \quad \Lambda_n = -\frac{\langle \mathbf{W}_{n-1}(i\hat{L} - \lambda_{n+1})\mathbf{W}_n\rangle}{\langle|\mathbf{W}_{n-1}|^2\rangle} \ ,$$

which were defined before by relationships (15). One can consider the set of the functions $M_n(t)$ together with the initial TCF ($n = 0$)

$$M_0(t) = a(t) = \frac{< \mathbf{A}_k^0(0)\mathbf{A}_{m+k}^m(t) >}{< |\mathbf{A}_k^0(0)|^2 >}, \quad t = m\tau,$$

as functions characterizing the statistical memory of the complex system with discrete time. The initial TCF $a(t)$ and the set $M_n(t)$ of discrete memory functions appearing from Eqns.(19) are playing an important role for the description of non-Markov and long-range memory effects. Now it is convenient to rewrite the set of Eqns. (19) as the chain of the couplednon-Markov discrete equations for initial discrete TCF $a(t)$ $(t = m\tau)$ and represent them in the form

$$\frac{\Delta a(t)}{\Delta t} = \lambda_1 a(t) - \tau\Lambda_1 \sum_{j=0}^{m-1} M_1(j\tau)a(t - j\tau),$$
$$\frac{\Delta M_1(t)}{\Delta t} = \lambda_2 M_1(t) - \tau\Lambda_2 \sum_{j=0}^{m-1} M_2(j\tau)M_1(t - j\tau),$$
$$\frac{\Delta M_2(t)}{\Delta t} = \lambda_3 M_2(t) - \tau\Lambda_3 \sum_{j=0}^{m-1} M_3(j\tau)M_2(t - j\tau). \tag{20}$$

The kinetic finite-difference Eqns. (19) and (20) are analogous to the well-known chain of kinetic equations of the Zwanzig'-Mori's type. These equations are playing a fundamental role in the modern statistical mechanics of nonequilibrium phenomena with continuous time. One can consider the kinetic equations (20) as a discrete-difference analogy of hydrodynamic equations for physical phenomena with discrete time. On the basis of the initial set of the experimental data one can find the set of orthogonal variables $\mathbf{W_n}$ in the following way

$$\hat{\mathbf{W}}_0 = \mathbf{A}_k^0, \quad \hat{\mathbf{W}}_1 = \left(\frac{\Delta}{\Delta t} - \lambda_1\right)\mathbf{A}_k^0,$$
$$\hat{\mathbf{W}}_2 = \left(\frac{\Delta}{\Delta t} - \lambda_2\right)\mathbf{W}_1 + \Lambda_1\mathbf{A}_k^0 = \{\left(\frac{\Delta}{\Delta t}\right)^2 - \frac{\Delta}{\Delta t}(\lambda_1 + \lambda_2) + \lambda_1\lambda_2 + \Lambda_1\}\mathbf{A}_k^0,$$
$$\hat{\mathbf{W}}_3 = \left(\frac{\Delta}{\Delta t} - \lambda_3\right)\mathbf{W_2} + \Lambda_2\left(\frac{\Delta}{\Delta t} - \lambda_1\right)\mathbf{A}_k^0. \tag{21}$$

It seems to us that one could suggest more physical interpretation of different terms in the right side of the three Eqs. (21). For example, term $\frac{\Delta A}{\Delta t}$ can be associated with dissipation, term $\frac{\Delta^2 A}{\Delta t^2}$ is similar to inertia and term $\Lambda_1 A(t)$ is related to restoring force. Then the third finite-difference derivative $\frac{\Delta^3 A}{\Delta t^3}$ is associated with the finite-difference form of the Abraham-Lorenz force corresponding to dissipation feedback due to radiative losses as seen from recent experimental evidence in frictional systems [11].

In concrete applications it is necessary to take into account that the dimension of new state vectors $\mathbf{W}_n$ is gradually decreasing with the increase of the number n. If the initial vector $\mathbf{A}_k^0$ has dimension the k then the vectors $\mathbf{W}_1$, $\mathbf{W}_2$ and $\mathbf{W}_3$ will have the dimensions $k-1$, $k-2$ and $k-3$, correspondingly.

Solving the chain of Eqns. (19) under the assumption that all $\lambda_s = 0$ one can find recurrence formulae for memory functions of arbitrary order in the following form

$$M_s(m\tau) = -\sum_{j=0}^{m-1} M_s(j\tau)M_{s-1}((m+1-j)\tau) + \varepsilon_s^{-1}\{M_{s-1}((m+1)\tau) - M_{s-1}((m+2)\tau)\}, \tag{22}$$
$$\varepsilon_s = \tau^2\Lambda_s, \ s = 1, 2, 3, \cdots.$$

By analogy with [11] it is convenient to define the generalized non-Markov parameter for frequency-dependent case as follows

$$\epsilon_i(\omega) = \left\{\frac{\mu_{i-1}(\omega)}{\mu_i(\omega)}\right\}^{\frac{1}{2}}, \tag{23}$$

where $i = 1, 2, ,$ and $\mu_i(\omega)$ is the power spectrum of the i-th memory function. It is convenient to use this parameter for quantitative description of long-range memory effects in the system considered together with memory functions defined above.

The set of new parameters describes the discrete structure of the system considered and allows to extract additional information related to non-Markov properties of the complex (non-Hamilton) systems .

III. LOCAL HURST DIMENSION ANALYSIS OF SEISMIC DATA

The Hurst exponent. Typical seismic data are seismic waves registration written in the form of vibrations of the Earth surface. Many observations as seismograms lead to random series registrations: technogenic noises, gravimetrical, economical, meteorological and other data. Some properties of such random series can be characterized by the Hurst exponent H [19], [20]. Let ξ_i define the i-th value of the observable variable, $<\xi_\tau>$ define its mean value on the segment containing τ registered points. For the cumulative average value we have $X(t,\tau)=\sum_{i=1}^{t}(\xi_i - <\xi>_r)$. The range R for the given sampling of the random series considered is defined as follows

$$R(\tau) = maxX(t,\tau) - minX(t,\tau), \tag{24}$$

at $1 < t < \tau$, where t is discrete time accepting integer values and τ is a length of the time sampling considered.

Normalizing the range R on the standard deviation S for the chosen sampling ξ_i

$$S(\tau) = \left(\frac{1}{\tau}\sum_{i=1}^{\tau}\{\xi(t) - \langle\xi\rangle_\tau\}^2\right)^{1/2} \tag{25}$$

and analyzing the variations of the normalized range Hurst [19], [20] obtained the following empirical relationship:

$$\frac{R(\tau)}{S(\tau)} = \tau^H, \tag{26}$$

where R is the range, S is the normalized variance and H is the so-called Hurst exponent for the sampling of the given length ξ. The value $H = 0.5$ corresponds to the normal distribution sampling, other values correspond to the various degrees of correlations, which can be interpreted in the terms of persistent coefficient. One can use the normalized range method for the definition of the Hurst exponent, but it works well for large samplings containing 1000-10000 registered points.

The calculation of the Hurst exponent for seismic data. One can obtain easily the Hurst exponent for long ($1000-10000$ registered points) samplings [21] by means of the method of the normalized range (R/S analysis). The Hurst exponent restoration accuracy calculated on the model data is located in the interval (0.1-1%). For example, if the model Hurst exponent was chosen as 0.7 then in the result of the R/S analysis the restored value is equaled to 0.69 with the changeable third decimal point. The calculated Hurst exponent for the initial seismic noise without an "event" (earthquake/explosion) accepted the values $0.96-0.98$. The obtained values show the high level of persistency and correlation. However, these values can be referred to the whole series and cannot reflect the peculiarities of the event. In other words, the values of the Hurst exponents calculated for the whole series cannot provide information about possible EQ's/TE's, which can be characterized by other values of persistency. In this situation it is necessary to generalize this parameter and define the notion of local Hurst exponent.

The local Hurst exponent. The generalized (local) Hurst exponent can be a sensitive indicator, which gives additional information about the regular component in the sampling considered. But the reason for changing of the Hurst exponent H is not only the presence of the signal in the sampling considered but slow (for natural processes) variations of the correlated noise itself.

If one considers random series for a relatively long time it is logically appropriate to cut the series into short segments and calculate the Hurst exponent H for each of them. In such a manner, one can detect the variations of H on time or in some spatial coordinates. It is better to use the shortest intervals possible for calculating the local exponent $H(t)$. $Sufficient$ number of registered points can serve as a criterion for choosing the minimal interval for such kind of statistical calculation of the local exponent H. So by analogy with conventional definition of the local temperature in statistical physics one can generalize the conception of the Hurst exponent and use it for short samplings. The reasons for changing of the Hurst exponents can be the following: a) slow changing of type of correlations inside the noises; b) the presence of the regular signal inside the noises. So, in concrete applications the local Hurst exponent can serve as a *quantitative* characteristic reflecting the fractal properties of the EQ or TE event. It is obvious that the usage of long intervals (1000 registered points and more) for the calculation of the local Hurst exponents becomes useless and the important question is choosing the acceptable interval for calculating this parameter with high accuracy. The usual R/S analysis does not give the acceptable accuracy for the local Hurst exponent related to short samplings containing $100-120$ points. So it is necessary to change the method of calculation of the local Hurst exponent for short samplings. The reliable calculation of the Hurst exponent averaged over short samplings turned out to be a nontrivial procedure and required elaboration of stable algorithms adjusted for averaging of short segments of the given samplings.

We used another definition for the Hurst exponent [21], which turned out to be more effective for short samplings. The best results have been achieved in the usage of expression for the normalized dispersion, which relates differences of a random function to retardation time τ:

$$V(\tau) = \frac{\langle (B_H(t+\tau) - B_H(t))^2 \rangle}{\langle B_H^2(t) \rangle} = \tau^{2H}, \tag{27}$$

here $B_H(t) = \sum_{i=1}^{t} \xi_i$, is an integral random function. As a the result of numerical experiments it has became possible to calculate the local Hurst exponent with acceptable accuracy ($4-5$ decimal points) for samplings containing about $80-120$ registered points.

IV. NON-MARKOV DISCRETE ANALYSIS OF SEISMIC DATA

Here we will apply the discrete non-Markov procedure developed in the previous Section 2 for the analysis of the real seismic data. The basic problems, which we are trying to solve in this analysis, are the following. The first problem relates to a possibility of seismic activity description by statistical parameters and functions of non-Markov nature. The second problem relates to distinctive parameters and functions for differentiation of weak EQ's (with small magnitudes) from TE's. The third problem is the most important one and relates to strong EQ's forecasting. With this aim in mind we analyzed three parts of the real seismogram: before the event (EQ and TE), during the event and after the event. A typical seismogram contains 4000 registered points. The complete analysis includes the following information: phase portraits of junior dynamical variables, power spectra of four junior memory functions and three first points of statistical spectrum of non-Markovity parameter. We took into account also the values of numerical parameters characterizing the seismic activity. To analyze time functions we used also the power spectra obtained by the fast Fourier transform. The complete analysis exhibits great variety of data.

We used 4 types of available experimental data courteously given by Laboratory of Geophysics and Seismology (Amman, Jordan) for the following seismic phenomena: strong EQ in Turkey (I) (summer 1999), a weak local EQ in Jordan (II) (summer 1998). As a TE we had the local underground explosion (III). The case (IV) corresponds to the calm state of the Earth before the explosion. All data correspond to transverse seismic displacements. The real temporal step of digitization τ between registered points of seismic activity has the following values, viz., $\tau = 0,02s$ for the case I, and $\tau = 0,01s$ for the cases II-IV. The graphical information is classified as follows:

Figs.1-6 are referred to the case I; Figs. 7,8 correspond to the cases II and III considered together; Figs.9,10 illustrate the case IV. At first we consider the figures, which were obtained from the recordings corresponding to the states defined as *before* and *during* strong earthquake (EQ). Figs.1(a,b,c,d) (before EQ, state Ib) and Figs.1(e,f,g,h) (during EQ, state I) demonstrate the temporal dynamics of four variables $W_0(t), W_1(t), W_2(t), W_3(t)$, which were calculated in accordance with Eqns. (14), (16). Let us note, that for convenience we use throughout initial variable $W_0(t)$ as a dimensionless variable. From these figures it follows that for variable W_0 the scale difference achieves the value more than 2500 (compare Figs.1a and 1e)! In comparison with the cases (1b,c) the figures (1f,g) reveal the long-range and low frequency oscillations for variables W_1 and W_2. One can calculate phase portraits in four-dimensional space of the obtained four dynamical variables W_0, W_1, W_2, W_3 as well. Figs. 2 and 3 show six projections on various two-dimensional planes of states: before (Figs. 2a,b,c, Figs. 3a,b,c) and during (Figs. 2d,e,f, Figs.3d,e,f) EQ.

The phase portraits of the system analyzed demonstrate strong variations. The last arise owing to the transformation of the strained state of the Earth before the EQ to the state during the EQ. The most dramatic changes emerge in the phase plane (W_1, W_0) (see Figs. 2a and 2d), plane (W_2, W_0) (Figs. 2b and 2e), plane (W_2, W_1) (Figs. 3b and 3e) and(W_3, W_1) (Figs. 3a and 3d). One can notice strong qualitative variations in the structure of phase portraits in the following planes: $(W_1, W_0), (W_2, W_0)$ and (W_2, W_1). Besides, we can see the quantitative change of space scales of dynamic orthogonal variables. The plane projection (W_0, W_1) remind a strange attractor. The changes of phase portraits in other planes are less noticeable (compare Figs. 2c and 2f, Figs 3b, 3c, 3e and 3f). The weakest change is revealed in the phase portrait in the plane (W_3, W_2). Probably, this phase portrait is less informative and encloses quasi-invariant part of the total phase portrait. Besides the spatial scales change of the orthogonal variables W_3 and W_2 , other essential deformations of this phase portrait were not observed.

As it has been mentioned above it is convenient to analyze the power spectra for comparison of memory functions. One can divide these spectra into the following regions: ultra-low frequency range (ULFR), low frequency range (LFR), middle frequency range (MFR) and high frequency range (HFR). Figs. 4 and 5 demonstrate spectra of four memory functions M_0, M_1, M_2, M_3 before and during EQ. Before (Fig. 4a) and during EQ (Fig.4c) the power spectrum of the initial TCF M_0 has a fractal form $1/\omega^{\alpha}$ in double-log scale. One can observe a peak in ULFR (Fig.4c) during EQ. The power spectra of the first and second memory functions during EQ (Figs. 4d and 5c) have also the fractal structure. The last one reflects the existence of linear frequency dependence in double-log scale within the LFR, MFR

and HFR. The similar fractal-like behavior for the Turkish strong EQ is preserved for the third memory function for the state during EQ (see Fig. 5d).

Figs. 6 demonstrates the power spectra of the first three points of the statistical spectrum of non-Markovity parameter for the states before (a, b, c) and during (e, f, g) strong the EQ. One can make the following conclusions from Figs. 6 a-d. On the first level of relaxation process (see, Fig. 6a) the strained state of the Earth crust before EQ can be associated with Markov and quasi-Markov behavior in ULFR and LFR, correspondingly. The influence of non-Markov effects is reinforced in MFR with $5 \cdot 10^{-2} f.u. < \omega < 10^{-1} f.u.$,$(1 f.u. = 2\pi/\tau)$. Strong non- Markovity of the processes considered for $\varepsilon_1(\omega)$ takes place in HFR with $10^{-1} f.u. < \omega < 0.5 f.u.$. Simultaneously we have the numerical values $\varepsilon_2(\omega), \varepsilon_3(\omega) \sim 1$ in the whole frequency region(see, Figs. 6 b, c). But this behavior implies that strong non-Markovity effects are observed in these cases.

The similar picture becomes unrecognizable for seismic state during the strong EQ (see, Figs. 6 d-f). Firstly, it is immediately obvious that $\varepsilon_1(\omega) \sim 1$ on first relaxation level.

Secondly, the second and third relaxation levels are non-Markovian (see, Figs. 6 e, f). Thus, the behavior of seismic signals during the strong EQ is characterized by strong non-Markovity on the whole frequency region.

Figs. 7 depicts power spectra of MF M_0 and M_1 for seismic states II and III. Figs. 8 shows power spectra of the first three points of non-Markovity parameter $\varepsilon_i(\omega), i = 1, 2, 3$. The preliminary results suggest that there is remarkable difference between weak EQ's and TE's especially in the area of low frequencies.

The analysis of the phase portrait for weak EQ's and underground TE's lead to the following conclusions. Firstly, these portraits cannot be differentiated. It can be seen from the range of spatial scales of the dynamical variables W_i and W_j and from the analysis of the phase points distribution forms. Secondly, it is necessary to remark some peculiarities in power spectra of $\mu_i(\omega)$, $i = 0, 1, 2, 3$ (see, Figs.8) for the cases II and III. All these spectra have distinctive similarities for the memory functions $M_i(t)$ with numbers $i = 0, 1, 2$ and 3. The character and the form of the spectra considered for the cases II and III are very similar to each other. The same similarity is observed for the three non-Markovity parameters $\epsilon_i(\omega)$, $i = 1, 2, 3$ (see, Figs. 8).

Nevertheless the analysis of the power frequency spectra allows to extract distinctive specific features between the weak EQ's and the TE's. Such quantitative criteria can be associated with frequency spectra of memory functions $\mu_i(\omega)$ characterizing the long-range memory effects in seismic activity. This new criterion allows to tell definitely a weak EQ from a TE, viz., to differentiate case II from case III.

A close examination of Figs. 8a and 8d shows that this distinction appear in frequency behavior of the first point of non-Markovity parameter $\varepsilon_1(\omega)$ close to the zero point $\omega = 0$. Specifically, the ratio of values $\varepsilon_1(0)$ for weak EQ and TE equal $\varepsilon_1^{II}(0)/\varepsilon_1^{III}(0) = 0.92/0.57 = 1.61$.

Let us to analyze the results of seismic activity characterizing the calm Earth state. Figs. 9,10 present the results of this analysis. They will be useful for the comparison with the results obtained for EQ's and TE's. The projections of the phase cloud on all six planes (W_i, W_j), $i \neq j$ exhibit approximately the similar distribution of phase points. The power spectra for the memory functions with the same parity (see, Figs.9) have a similar form. For example, for even order functions $\mu_0(\omega)$ and $\mu_2(\omega)$ one can notice sharp peaks near the frequency 0.2 $f.u.$ (see, Figs. 9a,c). In the spectrum of the senior function $\mu_2(\omega)$ (see Fig. 9c) additional peaks in HFR appears. One can notice two groups of characteristic peaks near $0.2 f.u.$ and $0.4 f.u$ in odd memory functions $\mu_1(\omega)$ and $\mu_3(\omega)$ (Figs. 9b, d). With the increase of order of the memory function the pumping over effect of peak intensities from the MFR to the HFR takes place. The frequency behavior of the three points of non-Markov parameters $\epsilon_1(\omega)$, $\epsilon_2(\omega)$ and $\epsilon_3(\omega)$ appeared to be practically the same. The behavior of the functions $\epsilon_i(\omega)$ exhibits the typical non-Markov character with small oscillations of random nature at LFR. The spectral characteristics of the system IV are very useful in comparison to the results obtained for the system I (before strong EQ).

Our observation shows that the zero point values of non-Markovity parameters for calm Earth state are equal $\varepsilon_1^{IV}(0) : \varepsilon_2^{IV}(0) : \varepsilon_3^{IV}(0) \approx 4.99 : 0.947 : 0.861$. These values are convenient for the comparison with similar values for the Earth seismic state before the strong EQ: $\varepsilon_1^{I}(0) : \varepsilon_2^{I}(0) : \varepsilon_3^{I}(0) \approx 214.3 : 0.624 : 0.727$. The change of ratio of the two first non-Markovity parameters $\varepsilon_1(0)/\varepsilon_2(0)$ is particularly striking . This ratio is equal to 5.27 for the calm Earth state, then it comes into particular prominence for the state before strong EQ: $\varepsilon_1^{I}(0)/\varepsilon_2^{I}(0) \approx 343.4$. Thus, this ratio changes approximately in 60 times! Hence, the behavior of this numerical parameter is operable as a reliable diagnostic tool for the strong EQ prediction. The foregoing proves that the indicated value drastically increases in process of nearing to strong EQ.

Finishing this Section, we give some preliminary suggestions relating to the strong EQs forecasting. They are related in comparison of frequency spectra obtained for the calm Earth (Figs. 11,12) and seismic activity data registered *before* a strong EQ (see, Figs. 2a,b,c; 3a,b,c; 4a,b; 5a,b and 6a,b). The comparison of the phase portraits demonstrates the following peculiarities. In the phase portraits calculated for the senior dynamical variables (W_2, W_1), (W_3, W_1) and (W_3, W_2) obtained for cases I and IV the distinctions are not noticeable (see Figs. 3a,b). These distinctions become noticeable in the phase portraits of junior variables (W_1, W_0), (W_2, W_0) and (W_3, W_0) (see, Figs. 2a,b,c). One can observe a gradual stratification of the phase clouds with the growth of elastic deformations before the strong

EQ. It is necessary to recall the double frequency difference for systems I and IV when comparing the frequency plots. The dependence $\mu_0(\omega)$, $\mu_1(\omega)$, $\mu_2(\omega)$ and $\mu_3(\omega)$ for systems I and IV (see Figs. 4a, b; 5a,b; and 14 a-d) is approximately similar, and qualitative difference is not noticeable. One can notice some visual difference only for two spectra: for the third memory function spectrum $\mu_3(\omega)$ and for the ULFR of the memory function $\mu_0(\omega)$. So the power spectra of memory functions can be used for the strong EQ forecasting. One can notice the similar changes in the behavior of the functions $\epsilon_1(\omega)$, $\epsilon_2(\omega)$ and $\epsilon_3(\omega)$ (see, Figs.6 a,b,c and 10 a,b,c). So one can conclude that careful investigations of frequency behavior of memory functions $\mu_i(\omega)$ and functions $\epsilon_i(\omega)$ describing the statistical non-Markovity parameters provide an accurate quantitative method of the strong EQ's forecasting. It is necessary to investigate carefully the power spectra with the accurate localization of an object and source, generating seismic signals, for further elaboration of this method.

For more complete understanding of non-Markov properties of seismic signals we give some kinetic parameters of our theory in Tables I-III. In Table I the full sets of kinetic parameters describing non-Markov stochastic processes in five various seismic states have been presented: before strong EQ(Ib), during strong EQ (I), during weak EQ (II), during TE (III) and for the calm Earth state (IV). The data cited in this Table are indicative of non-equilibrium properties (parameters λ_1, λ_2 and λ_3), long-range memory effects (parameters Λ_1 and Λ_2) and non-Markov peculiarities (parameters $\varepsilon_1(0), \varepsilon_2(0)$ and $\varepsilon_3(0)$). The differences under observation for various seismic states are sufficient to allow definite conclusions.

For purposes of clarity, Table II illustrates the of comparison of specific kinetic non-Markov parameters for two seismic state: before strong EQ(Ib) and calm Earth states (IV). As will be seen from Table II differences of parameters for these two states vary within a broad range: from 2.8 (parameter Λ_2) to 44.0 (for parameter $\varepsilon_1(0)$). Similarly, Table III contains comparison data for the other two seismic states: during weak EQ(II) and during underground TE(IV). Differences of parameters in this case are established within more narrow limits: from 2.486 (for parameter Λ_1) to 1.614 (for parameter $\varepsilon_1(0)$).

Thus, the existence of discreteness and long-range memory in behavior of seismic signals opens up new fields of use in the analysis of the Earth seismic activity. We can state with assurance that the differences under observation favor the view that the non-Markov parameters of our theory will be available for strong EQ's forecasting and differentiation of TE's from weak EQ's.

V. LOCAL HURST EXPONENT CALCULATIONS FOR AVAILABLE EARTHQUAKES AND TECHNOGENIC EXPLOSIONS DATA

Available data for the calculation of the local Hurst exponents contains 3000-5000 registered points describing the visible part of a wavelet. This number of the recorded points allows to use the procedure of the local Hurst exponent $H(t)$ calculation. For the realization of the procedure described in the previous Section 3 it is necessary to divide the whole sampling containing 25000 points into small intervals of 100-200 points, where the local Hurst exponent is supposed to be constant. On Fig. 11 we show a typical plot of the function $H(t)$ calculated for a typical EQ. The same features of $H(t)$ behavior are conserved for wide class of available weak EQ's. Then we obtained the calculated values of the local Hurst exponents $H(t)$ for available EQ's and explosions. Figs. 12 exhibits the typical behavior of these functions. The sharp decreasing (0.1) of the local Hurst function during "an event" is typical for explosions. Then the values of the function $H(t)$ are relaxing slowly to their initial values. For EQ's one can notice more gradual change of $H(t)$ before the event. The relaxation of $H(t)$ starts from higher (0.85) values and it comes back faster to its initial values in comparison with explosions. Such behavior is preserved for weak signals, when the ratio S/N decreases. For these cases the criterion of EQ or TE distinction is related to the amplitude of the Hurst exponent change during the analyzed event. It is necessary to increase the number of registered points per unit of real time in order to obtain a more distinctive picture, which can be more useful in differentiation of these events. It is related to the fact that the sensitivity of correlations of a random fractal value changing is associated with the lower temporal limit of the corresponding measurements. The smoothed change of $H(t)$ obtained for EQ's opens a possibility of more accurate registration of $H(t)$ before the visual wavelet of EQ's.

VI. CONCLUSION

We want to stress here again that these presented method have been applied successfully for differentiation of EQ's from TE's. We hope that the results of this analysis can be applied to a set of phenomena related with differentiation of similar signals of different nature. In the result of this analysis we received a new possibility to forecast of strong

EQ's approaching,analyzing only seismograms recorded for transverse seismic waves. Secondly, we received sufficient amount of information for the definite differentiation of weak EQ's from TE's.

In this paper we have presented the results of application of two new methods for the study of dynamic, kinetic and spectral properties of seismic signals depicting EQ's and TE's modulation. By the discrete non-Markov stochastic processes and the local Hurst exponent analysis we have found explicitly some features of several different states of the Earth crust: states of the the Earth *before* and *during* strong and weak EQ's, during TE's. The used methods allow to present the seismogram analyzed in the form of set non-Markov variables and parameters. They contain great amount of the qualitative and quantitative information about seismic activity.

The dynamic information is contained in time recordings of new orthogonal dynamic variables, different plane projections of the multidimensional phase portrait and the time dependence of local Hurst exponent. The information on the kinetic, spectral and statistical properties of the system is expressed through time dependence of the initial TCF, memory functions of junior orders, their power and frequency spectra of the first three points of statistical spectrum of non-Markovity parameter.

The main advantage of our two new methods is a great amount of supplementary information about the properties of seismic signals makes. The problem is its correct application. What kind of possibilities can one expect? It is possible to answer as follows. Firstly, our preliminary study, convincingly demonstrates that the relevant and valuable information on non-Markov and discrete properties of the system considered is contained in seismic signals. In all the studied systems (I- IV) we have found out unique manifestations of Markov, quasi-Markov and non-Markov processes on the particular behavior of the signals in a broad range of frequencies.

The similar results cannot be obtained, on principle, by other methods used in the analysis of seismic activity.

Secondly, in the non-linear non-Markov characteristics some of well-known spectral effects are evident. Among them the following effects are exhibited noticeably: fractal spectra with an exponential function $\omega^{-\alpha}$, which are connected to the phenomenon of usual (SOC) and restricted (RSOC) self-organized criticality [15,16], behavior of some frequency spectra in the form of white and color noises. Thirdly, the frequency spectra introduced above are characterized by the particular alternation of Markov (fractal) and non-Markov spectra (such as color or white noises). The similar alternation resembles in particular the peculiar alternation of effects of a non-Markov and non-Markov behavior for hydrodynamic systems in the statistical physics of condensed matter detected in papers [17], [18] for the first time. The fine specification of such alternation appears essentially different for studied states I-IV. These features allow to view optimistically the solution of the problem of forecasting strong EQ's and differentiation TE's from weak EQ's.

VII. ACKNOWLEDGEMENTS

We would like to thank our Referee for careful reading of the initial version of our manuscript presented, valuable remarks and well-wishing comments, which undoubtedly improved the quality of the paper. One of the authors (R.R.N) gratefully acknowledges Dr. Tawfiq Ch. Al-Yazjeen (Laboratory of Geophysics and Seismology, Amman, Jordan) for making possible access to some seismology data for their subsequent analysis. Authors thank Dr. L.O.Svirina for technical assistance.

This work partially supported by Russian Humanitarian Science Fund (Grant N 00-06-00005a) and NIOKR RT Foundation (Grant N 14-78/2000).

---

[1] D.Sornette and C. Sammis, *J. Phys. I (France)* **5**, 607 (1995).
[2] C.G.Sammis, D. Sornette, and H.Saleur,in *Reduction and Predictability of Natural Disasters* , edited by Rundle, Turcotte, and Klein, SFI Studies in the Sciences of Complexity **25** (Addison-Wesley, 1996), p. 143.
[3] J.-C. Anifrani, C. Le Floc'h, D.Sornette, and B. Souillard, *J. Phys. I (France)* **5**, 631 (1995).
[4] H. Saleur, C.G. Sammis, and D.Sornette, *J. Geophys. Res.* **101**, 17661 (1996).
[5] D.Sornette, A.Johansen, A.Arneodo, J.F.Muzy, and H.Saleur, *Phys.Rev.Lett.* **76**, 251 (1996).
[6] A. Johansen and D.Sornette, *Int. J. Mod. Phys.* **9**, 433 (1998).
[7] D. Sornette and L. Knopoff, *Bull. Seism. Soc. Am.* **87**, 789 (1997).
[8] B. K. Chakrabarti and R.B. Stinchcombe, *Physica A* **270**, 27 (1999).
[9] D.Sornette, *Phys. Rep.* **313**, 237 (1999).
[10] P.Yiou, D.Sornette, and M.Ghil, *Physica D* **142**, 254 (2000).
[11] R. Yulmetyev, P. Hänggi, and F. Gafarov, *Phys. Rev. E* **62**, 6178 (2000).

[12] P. Gaspard and X.-J. Wang, *Phys. Rep.* **235**, 291 (1993).
[13] A. Wehrl, *Rep. Math. Phys.* **30**, 119 (1991).
[14] M.Ausloos, N.Vandewalle, Ph.Boveroux, A.Minguet, and K.Ivanova, *Physica A* **274**, 229 (1999);
A.-L.Barabási and T.Vicsek, *Phys.Rev.A* **44**, 2730 (1991);
A.Marshak, A.Davis, R.Cahalan, and W.Wiscombe, *Phys.Rev.E* **49**, 55 (1994).
[15] P.Bak, C.Tang, and K.Wiesenfeld, *Phys. Rev.Lett.* **59**, 381 (1987);
P.Bak, C.Tang, and K.Wiesenfeld, *Phys.Rev.A* **38**, 364 (1988);
H.J.Jensen, *Self-organized criticality* (Cambridge University Press, Cambridge, England, 1998).
[16] S.-D.Zhang, *Phys. Rev. E* **61**, 5983 (2000);
C.Heneghan and G.Mc Darby, *Phys.Rev.E* **62**, 6103 (2000);
J.Davidsen and H.G. Schuster, *Phys. Rev.E* **62**, 6111 (2000);
S.Maslov, C.Tang and Y.-C.Zhang, *Phys. Rev.Lett.* **83**, 2449 (1999).
[17] R.M.Yulmetyev and N.R.Khusnutdinov, *J.Phys.A* **27**, 5363 (1994).
[18] R.M.Yulmetyev and N.R.Khusnutdinov, *Theoret.Math.Phys.* **105**, 292 (1995).
[19] H.E. Hurst, R.P. Black, and Y.M. Simaika, *Long-Term Storage: An Experimental Study* (Constable, London, 1965).
[20] H.E. Hurst , *Trans.Am.Soc.Civ. Eng.* **116**, 770 (1951).
[21] J.Feder, *Fractals, Chapter 8* (Plenum Press, New York and London 1988).

VIII. FIGURE CAPTIONS

Figure 1. The temporal dynamics of the first four dynamic variables $W_0(t)$, $W_1(t)$, $W_2(t)$, $W_3(t)$: a,b,c,d - before strong EQ, e,f,g,h - during of strong EQ. During strong EQ fluctuation scale increase drastically. It makes up: $2.5*10^3$ for initial variable $W_0(t)$,10^2 for the first orthogonal variable $W_1(t)$,10 for $W_2(t)$ and 2 for $W_3(t)$. The existent trend vanishes gradually at transition from the initial variable $W_0(t)$ to the third orthogonal variable $W_3(t)$. The fluctuation scale decreases sharply during the strong EQ.

Figure 2. The phase portrait projections on the planes of orthogonal variables W_0, W_1 (a), W_0, W_2 (b), W_0, W_3 (c)- before the strong EQ(Ib) and W_0, W_1 (d),W_0, W_2 (e), W_0, W_3 (f) during the strong EQ (I). The sharp difference is distinct for seismic states Ib and I. The randomization of the phase portrait for state I begins from plane W_0, W_2. Together with the difference of the scale of fluctuation, one can observe the asymmetric distribution of phase clouds everywhere.

Figure 3. The phase portrait projections on the planes of orthogonal variables W_1, W_2 (a), W_1, W_3 (b), W_2, W_3 (c)- before the strong EQ (Ib) and on planes W_1, W_2 (d),W_1, W_3 (e), W_2, W_3 (f) during of strong EQ (I). All phase clouds for seismic state Ib are symmetrical as opposed to Figs.2. Sharply marked asymmetry and stratification of phase clouds, what resembles known situation for myocardial infarction in cardiology, are observed for state I (d,e, and f).

Figure 4. The power spectra of the two first memory functions μ_0 and μ_1 : (a,b) -before the strong EQ(Ib), (c,d)- during of the strong EQ (I).For the cases a,c and d we observe fractality and self-organized criticality (SOC). SOC exists for the whole frequency range for state Ib. However, we observe restricted SOC at c and d cases only in frequency range down to $2.5 * 10^{-3}$ units of $(2\pi/\tau)$. Restricted SOC is characterized by sharp decreasing of intensity on two orders for c and d cases! One can see color noises nearby 0.1 and 0.2 f.u. for μ_1 in state Ib.

Figure 5. The spectra of two memory functions μ_2 and μ_3: (a,b) -before the strong EQ, (c,d)- and during the strong EQ. One can observe color noises in cases a,b and d. Fractal-like spectrum on ultra-low frequencies is appreciable in addition to cases c and d. The spectra for states Ib and I are sharply different from each other both to intensity and to spectral peaks positioning.

Figure 6. Frequency spectra of the first three points of non-Markovity parameters ϵ_1 ϵ_2, ϵ_3: (a,b,c)- before the strong EQ, (d,e,f)- during the strong EQ. Markov and quasi-Markov behavior of seismic signals is observed only for ϵ_1 in state Ib. All remaining cases (b,c,d and d) relate to non-Markov processes. Strong non-Markovity is typical for cases b , c (state Ib) and for case d (state I). In behavior of $\epsilon_2(\omega)$ and $\epsilon_3(\omega)$ one can see a transition from quasi-Markovity (at low frequencies) to strong non-Markovity (at high frequencies).

Figure 7. The power spectra for the two first memory functions μ_0 and μ_1: (a,b) -during weak EQ, (c,d)- during technogenic explosion. In cases Ib and I the spectra are characterized by strong differences especially on ultra low frequencies. They have very low intensity for μ_0 on low frequencies (cases a and c) and color like behavior for μ_1 for states II and III(cases b and d). Unexpected peaks exist in system III in LFR. Color and intensity distribution of the spectra is different for states II and III.

Figure 8. The frequency spectra of the first three points in statistical spectrum of non-Markovity parameters ϵ_1, ϵ_2, ϵ_3: (a,b,c)- during weak EQ, (d,e,f)- during TE . All spectra are characterized by strong expressed non- Markovity ($\epsilon_i \sim 1$) for the whole frequency range. Weak quasi- Markovity is observed near zero frequency for cases a and d (ϵ_1 vary from 0.5 up to 6.5). A noticeable difference for states II and III exists in behavior $\epsilon_1(\omega)$ in point $\omega = 0$. Due to this fact, one can develop reliable approach to differentiation between weak EQ's and underground TE's.

Figure 9. The power spectra of memory functions $\mu_0(\omega)$, $\mu_1(\omega)$, $\mu_2(\omega)$ and $\mu_3(\omega)$ for the calm state of the Earth before explosion. All functions $\mu_i(\omega)$, $i = 0, 1, 2, 3$ have approximately similar fractal behavior with restricted SOC and color noises close to 0.2 and 0.4 f.u. The maximum of intensity emerges close to the frequency $4 * 10^-3 f.u.$. A slight change and redistribution of intensity of power spectra occur with the increase of order of memory function.

Figure 10. The power spectra of the first three points in statistical spectrum of non-Markovity parameter ϵ_1, ϵ_2, ϵ_3 for calm state of the Earth before explosion(IV). Due to similar frequency behavior of all memory functions $\mu_i(\omega)$ the functions $\epsilon_i(\omega)$, i=1,2 and 3 have approximately similar frequency behavior and therefore demonstrate strong non-Markovity on all levels. The initial parameter $\epsilon_1(\omega)$ is non-Markovian with the exception of slight quasi-Markovity close to low frequencies below 0.1 f.u. As a result of this the possibility appears for forecasting the strong EQ's by registration of disappearance of strong non-Markovity and appearance of pronounced Markov time effects.

Figure 11. The typical temporal behavior of the Hurst exponent $H(t)$ calculated for EQ's. One can see sharp decreasing of $H(t)$ on 15 % during EQ. After that a gradual restore of the Hurst exponent $H(t)$ to normal value ≈ 1 takes place.

Figure 12. The comparative analysis of the Hurst exponent $H(t)$ behavior during the weak EQ (a,c) and for the TE (b,d). During the weak EQ's one can see sharp decreasing of $H(t)$ on 15 % and almost 90 % during the TE. These observations enable us to develop a new approach to differentiation the TE's from weak EQ's.

Table I. Set of kinetic non-Markov parameters of discrete stochastic processes in various seismic states

	before strong EQ, Ib	during strong EQ, I	during weak EQ, II	during TE, III	calm state of Earth, IV
λ_1, units of τ^{-1}	-0.0052275	-0.00010709	-0.32465	-0.17203	-0.22972
λ_2, units of τ^{-1}	-0.61788	-0.00058654	-0.81717	-0.84403	-0.96049
λ_3, units of τ^{-1}	-0.85737	-0.20212	-1.0147	-1.0076	-0.99313
Λ_1, units of τ^{-2}	0.0040768	0.00011576	0.14726	0.059232	0.021134
Λ_2, units of τ^{-2}	0.31541	4.5948e-005	-0.034187	-0.032079	0.11266
$\varepsilon_1(0)$	214.3	1.52	0.92	0.57	4.99
$\varepsilon_2(0)$	0.624	8.67	1.02	1.008	0.947
$\varepsilon_3(0)$	0.727	6.77	1.02	1.007	0.861
$\tau(s)$	0.02	0.02	0.01	0.01	0.01

This figure "fig2.jpg" is available in "jpg" format from:

http://arXiv.org/ps/cond-mat/0111453v1

Table II. Comparison of kinetic non-Markov parameters for two seismic states: before strong EQ (Ib) and calm Earth state (IV)

ratio of parameters	$\varepsilon_1^{Ib}(0)/\varepsilon_1^{IV}(0)$	$\lambda_1^{Ib}/\lambda_1^{IV}$	$\Lambda_1^{Ib}/\Lambda_1^{IV}$	$\Lambda_2^{Ib}/\Lambda_2^{IV}$
numerical value	42.94	1:22.0	1:1.3	1:0.7

This figure "fig3.jpg" is available in "jpg" format from:

http://arXiv.org/ps/cond-mat/0111453v1

Table III. Comparison of kinetic non-Markov parameters for two seismic states: during weak EQ (II) and during underground TE (III)

ratio of parameters	$\Lambda_1^{II}/\Lambda_1^{III}$	$\lambda_1^{II}/\lambda_1^{III}$	$\varepsilon_1^{II}(0)/\varepsilon_1^{III}(0)$
numerical value	2.486	1.887	1.614

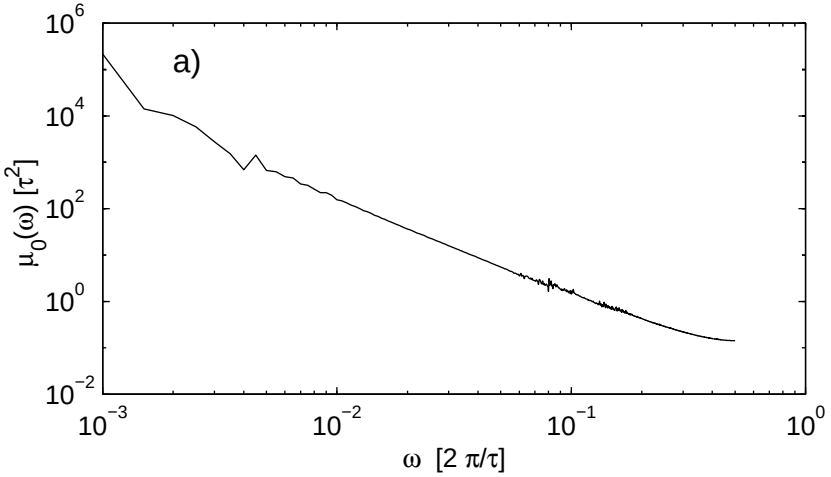
a)
10^6
10^4
10^2
10^0
10^{-2}
$\mu_0(\omega)$ [τ^2]
10^{-3}
10^{-2}
10^{-1}
10^0
ω [2 π/τ]

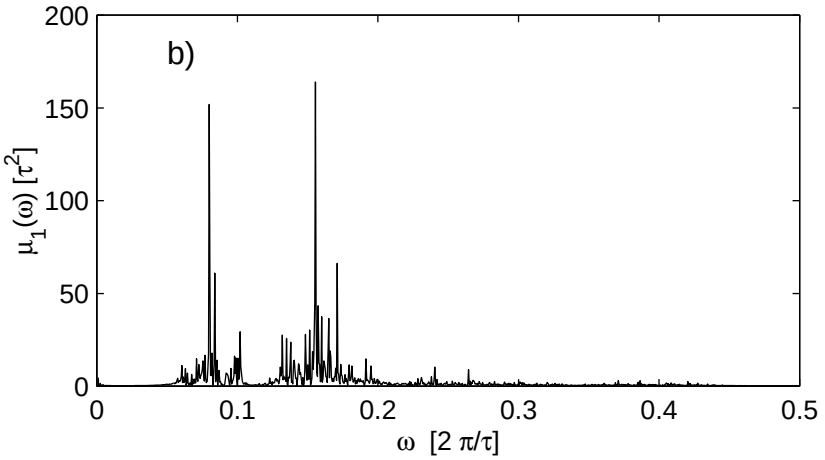
b)
200
150
100
50
0
$\mu_1(\omega)$ [τ^2]
0
0.1
0.2
0.3
0.4
0.5
ω [2 π/τ]

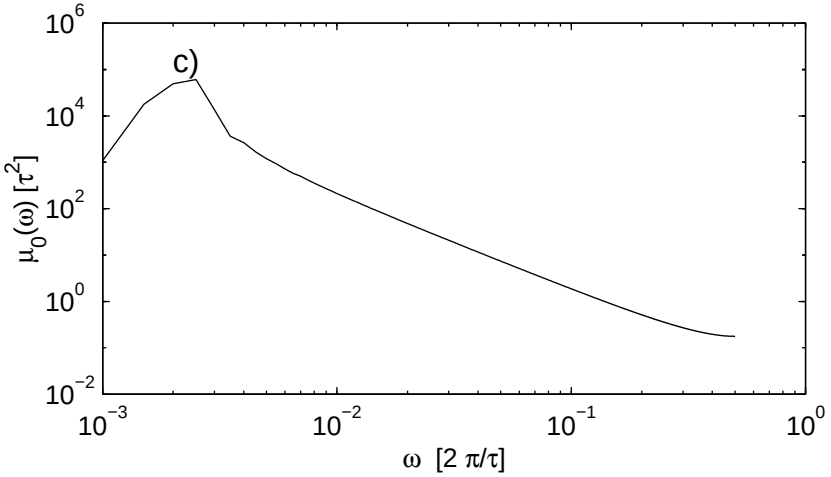
c)
10^6
10^4
10^2
10^0
10^{-2}
$\mu_0(\omega)$ [τ^2]
10^{-3}
10^{-2}
10^{-1}
10^0
ω [2 π/τ]

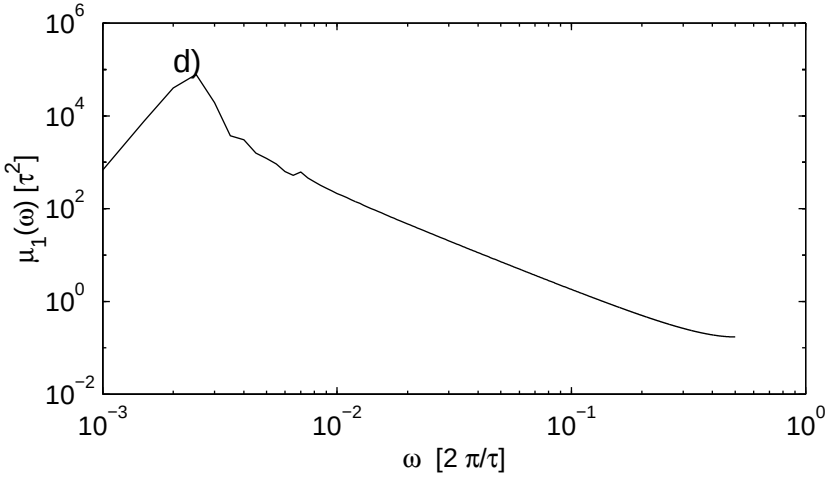
d)
10^6
10^4
10^2
10^0
10^{-2}
$\mu_1(\omega)$ [τ^2]
10^{-3}
10^{-2}
10^{-1}
10^0
ω [2 π/τ]

Figure 4

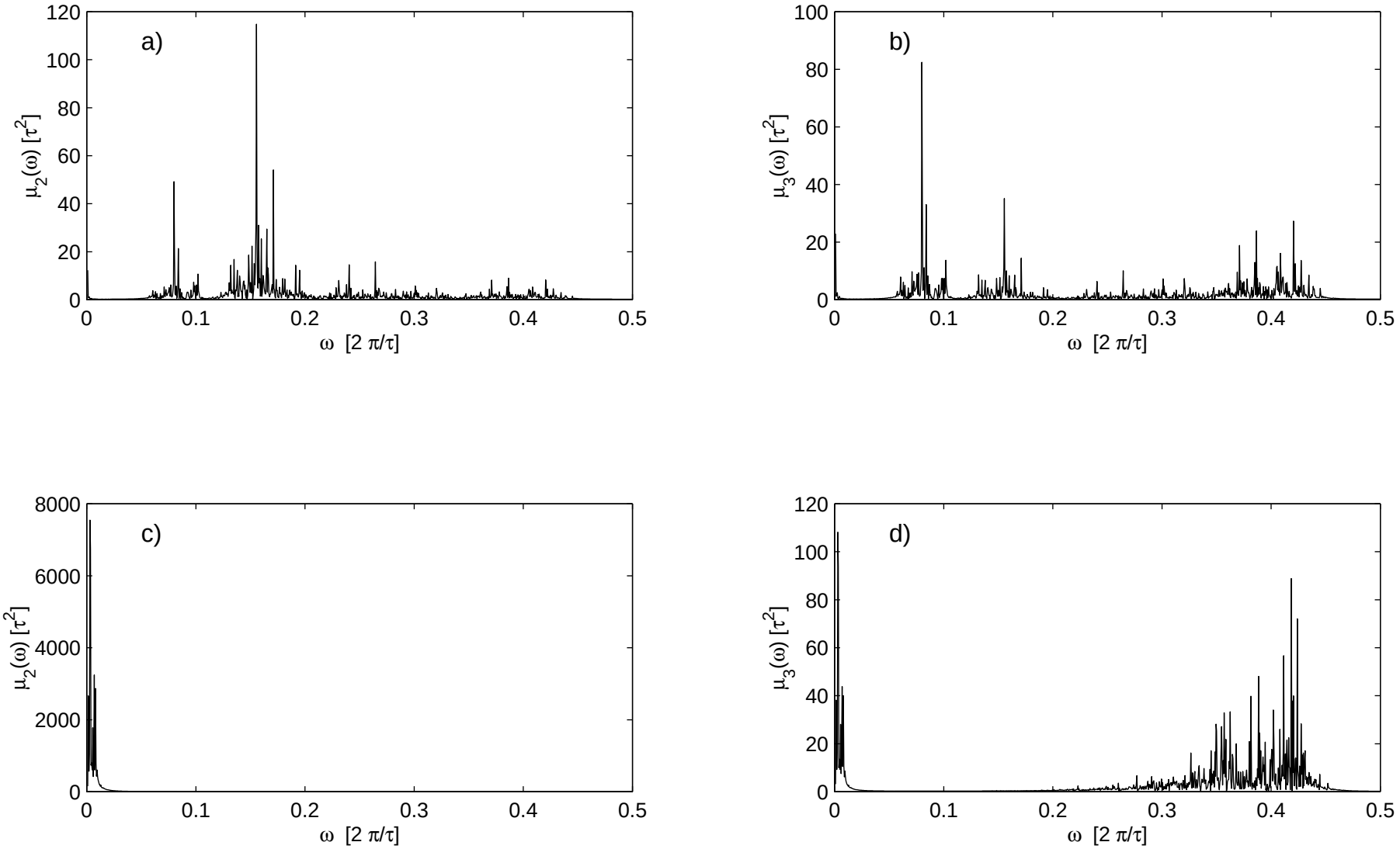

Figure 5

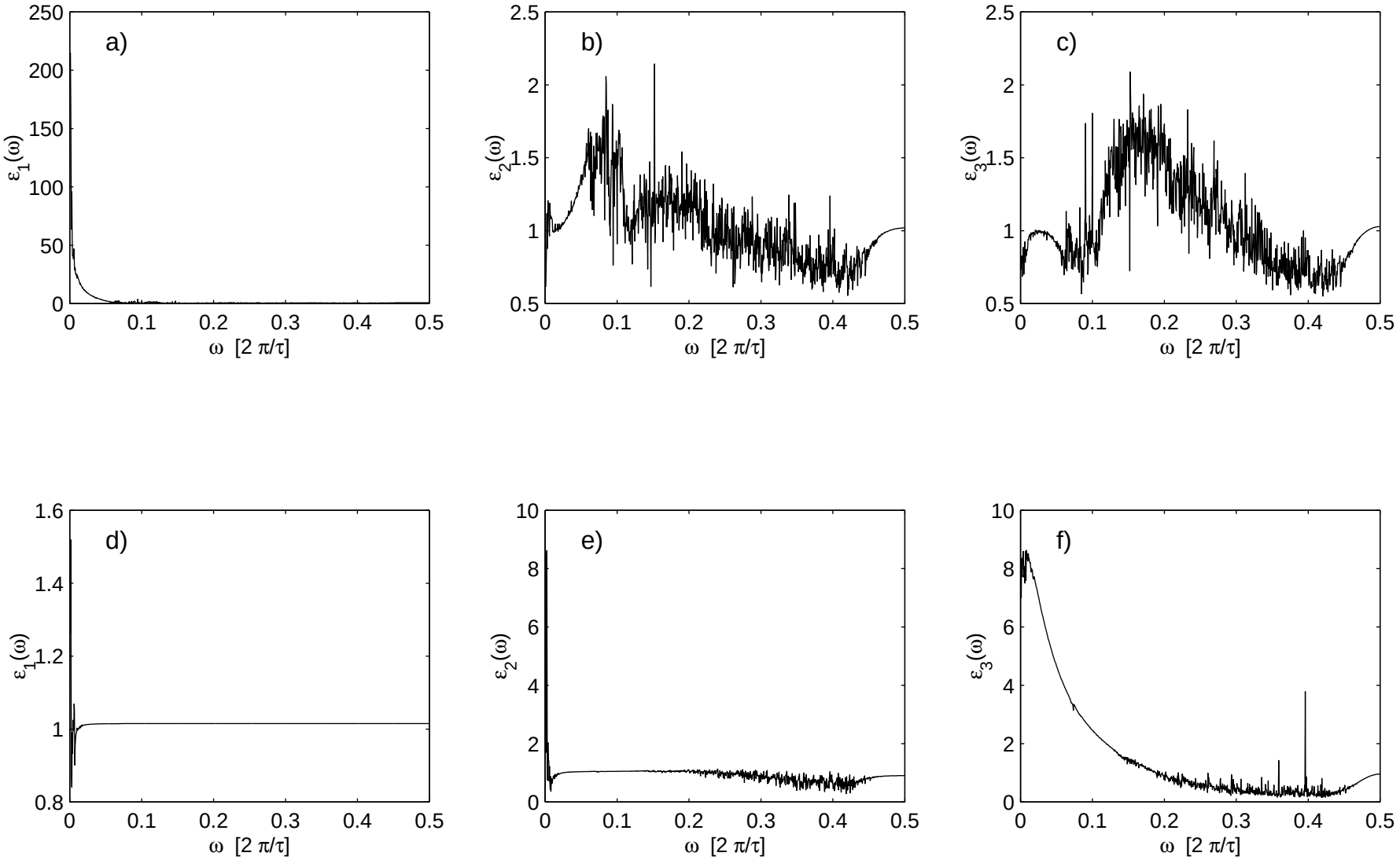
a)
b)
c)
d)
e)
f)
$\varepsilon_1(\omega)$
$\varepsilon_2(\omega)$
$\varepsilon_3(\omega)$
ω [2 π/τ]

Figure 6

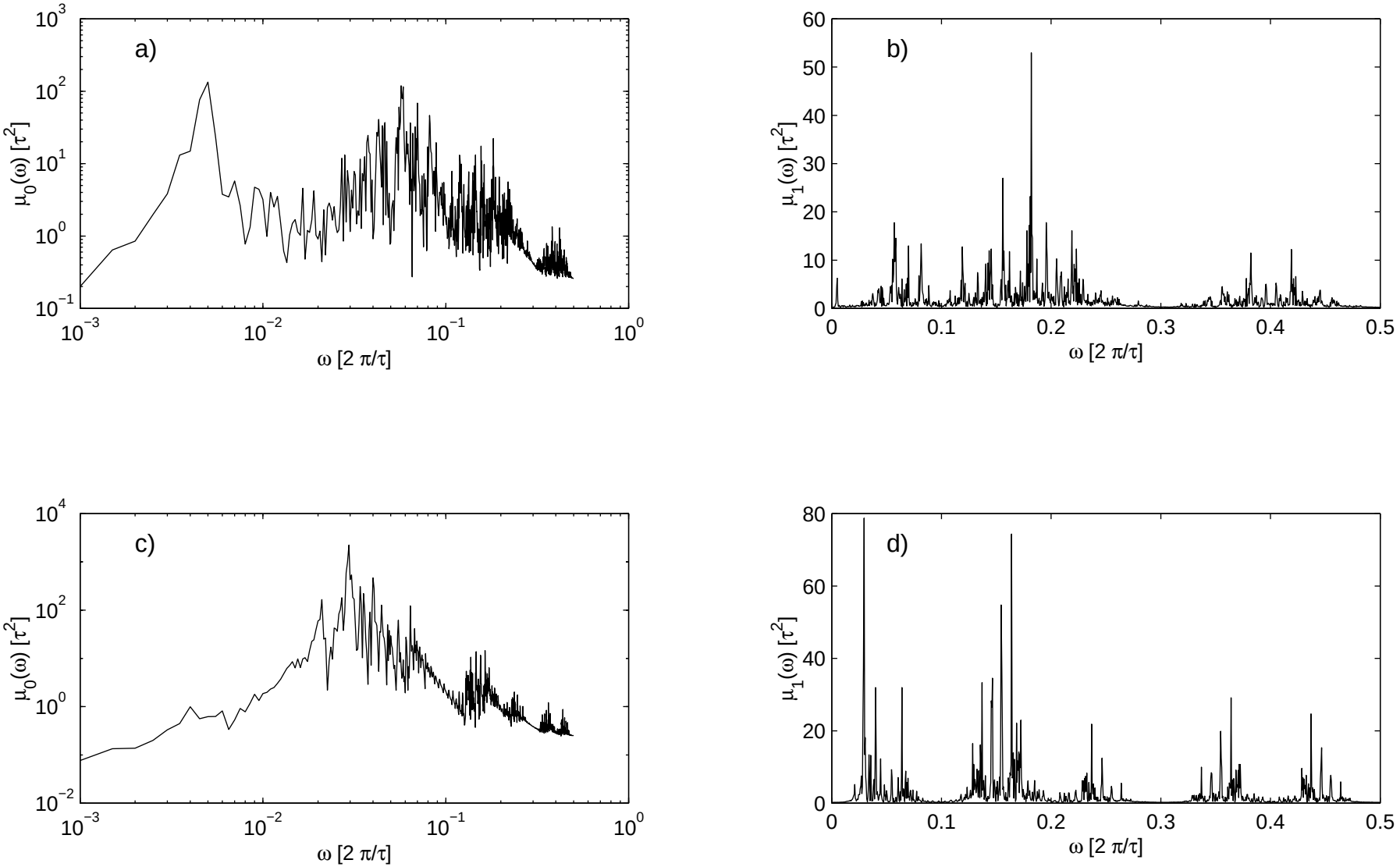

Figure 7

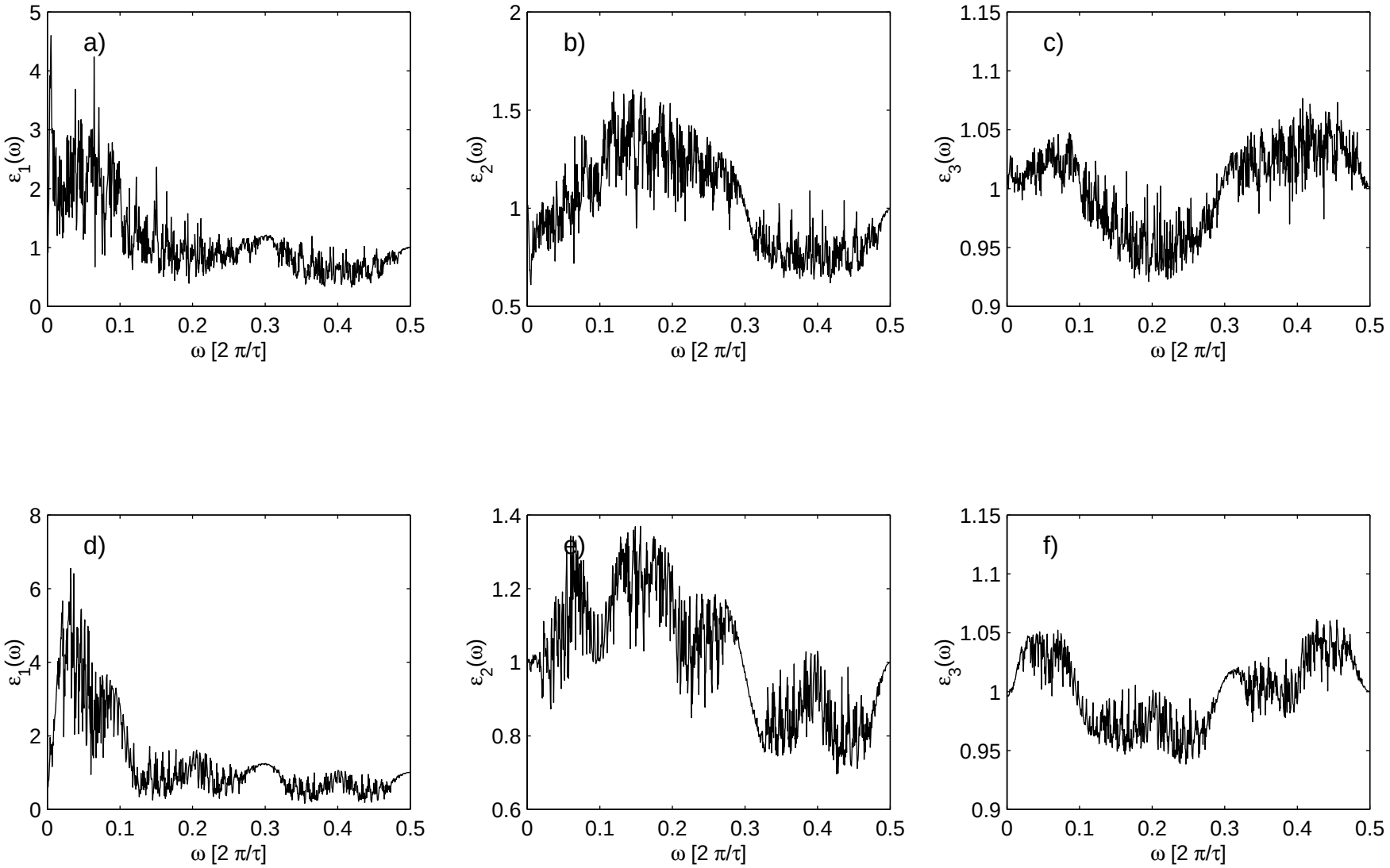

Figure 8

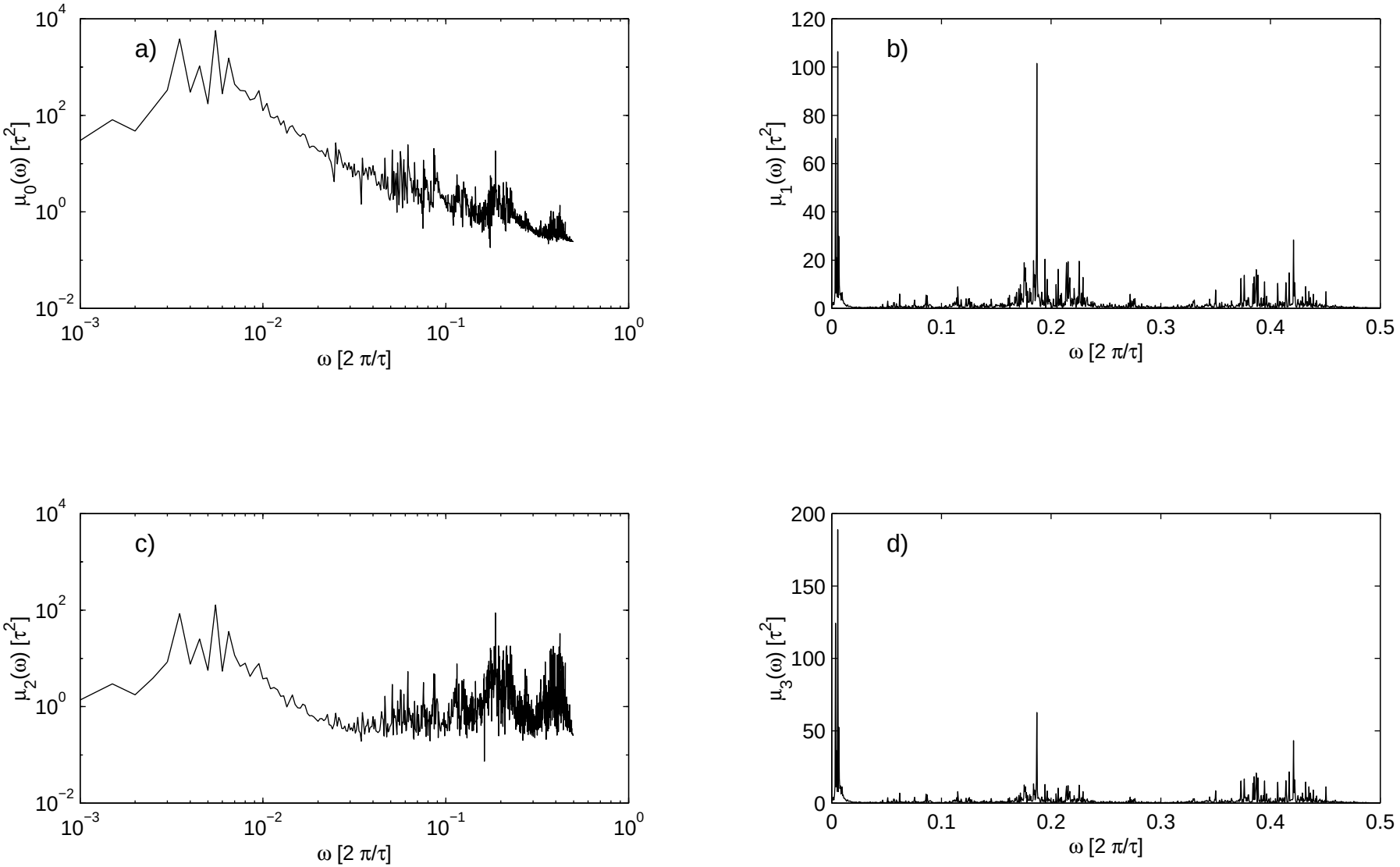
a)
b)
c)
d)
$\mu_0(\omega)$ [τ^2]
$\mu_1(\omega)$ [τ^2]
$\mu_2(\omega)$ [τ^2]
$\mu_3(\omega)$ [τ^2]
ω [2 π/τ]
10^{4}
10^{2}
10^{0}
10^{-2}
10^{-3}
10^{-1}
120
100
80
60
40
20
0
0.1
0.2
0.3
0.4
0.5
200
150
50

Figure 9

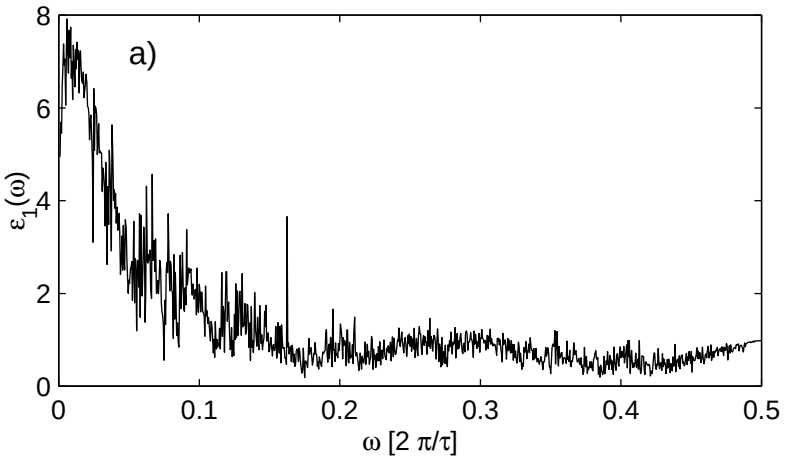
a)
8
6
4
2
0
$\varepsilon_1(\omega)$
0
0.1
0.2
0.3
0.4
0.5
ω [2 π/τ]

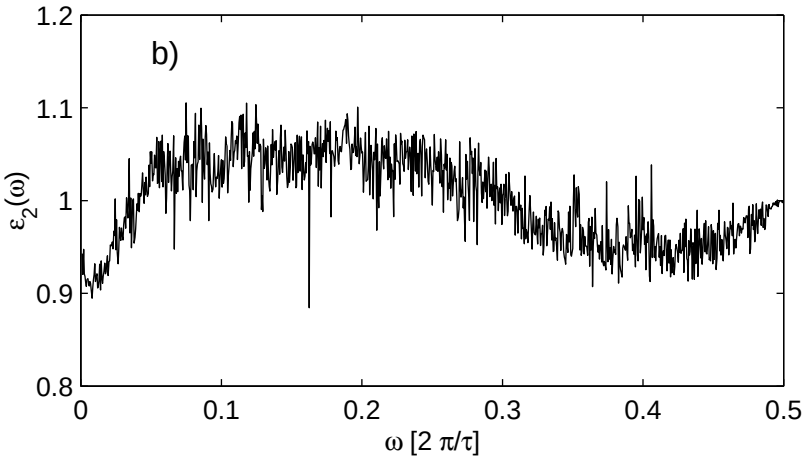
b)
1.2
1.1
1
0.9
0.8
$\varepsilon_2(\omega)$
0
0.1
0.2
0.3
0.4
0.5
ω [2 π/τ]

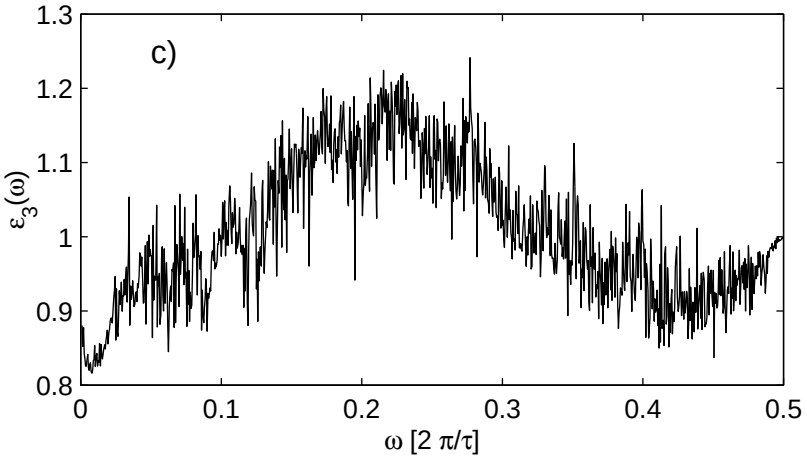
c)
1.3
1.2
1.1
1
0.9
0.8
$\varepsilon_3(\omega)$
0
0.1
0.2
0.3
0.4
0.5
ω [2 π/τ]

Figure 10

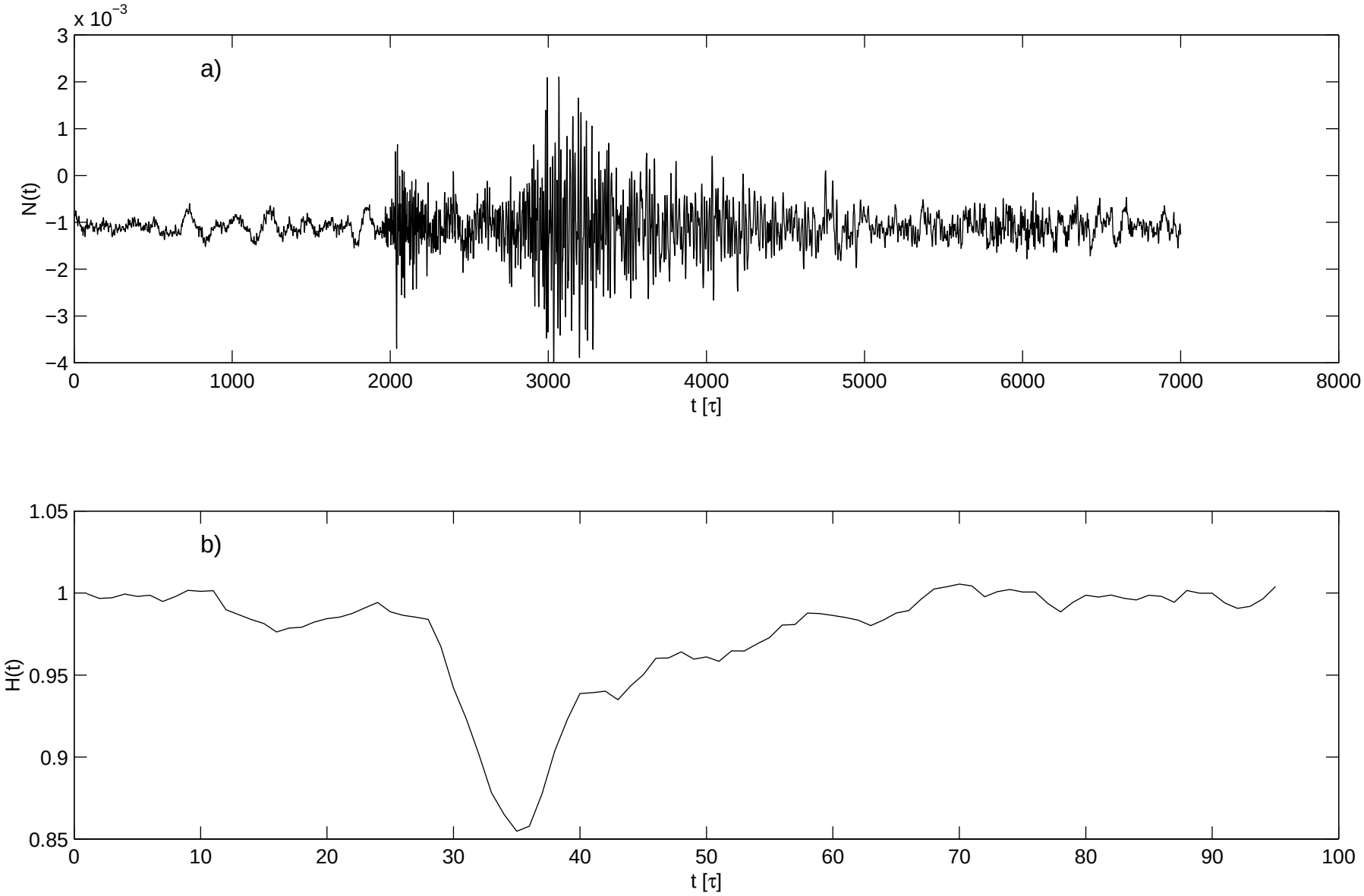

Figure 11

This figure "fig12.jpg" is available in "jpg" format from:

http://arXiv.org/ps/cond-mat/0111453v1